Journal of Alloys and Compounds 509 (2011) 2684–2692

Contents lists available at ScienceDirect

Journal of Alloys and Compounds

journal homepage: www.elsevier.com/locate/jallcom

Mechanical behaviors of Ti–V–(Al, Sn) alloys with α′ martensite microstructure

Hiroaki Matsumoto[a,*], Hiroshi Yoneda[b], Damien Fabregue[c], Eric Maire[c], Akihiko Chiba[a], Fumihiko Gejima[d]

[a] Institute for Materials Research, Tohoku University, Metallic Glass Center, 2-1-1 Katahira, Aobaku, Sendai 980-8577, Japan
[b] Tohoku University, Japan
[c] Université de Lyon, INSA LYON, CNRS, Mateis, France
[d] Nissan Motor Co., Ltd, Japan

ARTICLE INFO

Article history:
Received 15 September 2010
Received in revised form 9 November 2010
Accepted 11 November 2010
Available online 21 November 2010

Keywords:
Titanium–vanadium–(aluminum or tin) alloy
Alpha prime martensite
Young's modulus
Deformation behavior

ABSTRACT

The mechanical properties and deformation behavior of Ti–V–(Al, Sn) alloys with a α′ martensite microstructure are examined in this work. In as-quenched Ti–V–Al alloys consisting of α′ martensite microstructure with compositions near α − (α + β), the cold-rolling ability drastically decreases from a reduction of more than 75% to less than 40% with an increase in Al content. While, excellent cold-rolling ability (more than 75% reduction) is seen in the constituent phases of α′ in the compositional region near β − (α + β), and α″ and β. On the other hand, in as-quenched Ti–V–Sn alloys, excellent cold-rolling ability with a reduction of more than 80% that is independent of phase constituents is seen. In α′ martensite Ti–V–Al–Sn alloy with compositions in α − (α + β) that is tensile-deformed at a strain of 5%, a homogenous deformation substructure with straight dislocations is seen in alloy that with a low Al content. In contrast, the dislocation substructure begins to exhibit a planar configuration with increasing Al content. This change in deformation substructure due to increasing Al content is considered to cause the low ductility in α′ martensite Ti alloy that contains high Al. On the other hand, in α′ martensite Ti–V–Al alloy with a composition near β − (α + β), plastic deformation is found to be proceeded via the activation of the basal ⟨*a*⟩ slip and the $\{10\bar{1}1\}$ twin with a homogenous deformation substructure. As a consequence, this deformation mode is considered to cause the high ductility in the α′ phase as compared with the equilibrium (α + β) phase.

1. Introduction

Ti alloys are widely used in industrial applications due to their excellent mechanical properties combined with low density. In particular, a Ti–V–Al alloy system, such as Ti–6Al–4V, Ti–6Al–6V–2Sn and others, is most widely used as an industrial Ti alloy. In general, Ti alloys are classified as α, α + β, and β alloys, with further subdivision into near α – and metastable β alloys. In (α + β)-Ti alloys, the alloy-type can be further subdivided into near α-type and near β-type depending on alloy composition whether it is close to α-type or β-type. Metastable β alloys belong to near β − (α + β) type alloy. The microstructures of Ti alloys, which can be controlled by hot forging and heat treatment, are well known to strongly influence on their mechanical properties. The microstructures obtained from supratransus solution treatment depend on the degree of homogenization during solution treatment and the cooling rate from the β field. Quenching suppresses the diffusion-controlled β(B.C.C.)-to-α(H.C.P.) transformation and leads to a martensitic transformation in which the β phase becomes needle-like α′(H.C.P.) martensite or α″ (orthorhombic) martensite, depending on the alloy content.

We have recently presented new types of Ti–V alloys that are composed of fully α′ martensite, with a low Young's modulus and high strength [1,2] for industrial applications such as screw and suspension springs. By optimizing the alloy content, this α′ martensite-type Ti–V alloy exhibits excellent cold-rolling ability of more than 90%. These results suggest that this new type of α′ martensite Ti alloy can be expected to replace the typical α, α + β and β Ti alloys.

So far, the α′ martensite has been utilized for microstructural control of the nucleation sites of α in (α + β) Ti alloy, though this microstructural control is not so common in the industrial production of Ti alloy [3]. Therefore, there have been few reports that systematically examine the characteristics of the martensite (α′ or α″) phase in Ti alloys in relation to mechanical properties. In this study, a systematic evaluation of the microstructures and mechanical properties of Ti–V–(Al, Sn) alloys with a α′ martensitic structure is conducted with changing alloying content and heat treatment conditions.

* Corresponding author. Tel.: +81 22 215 2118; fax: +81 22 215 2116.
E-mail address: matumoto@imr.tohoku.ac.jp (H. Matsumoto).

0925-8388/$ – see front matter © 2010 Elsevier B.V. All rights reserved.
doi:10.1016/j.jallcom.2010.11.089

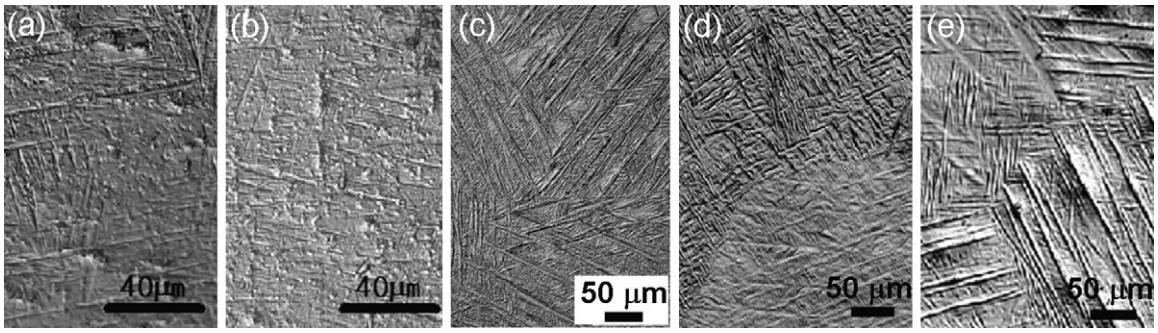

Fig. 1. Optical micrographs of STQ alloys of (a) (Ti–4%V)–1%Al, (b) (Ti–4%V)–4%Al, (c) (Ti–12%V)–2%Al, (d) (Ti–8%V)–4%Sn, and (e) (Ti–12%V)–6%Sn.

The Al and the Sn are well recognized as major alloying elements in Ti–V based alloy due to the effects of strengthening of the alloy and suppression of ω-phase formation. Therefore, three kinds of alloy systems of Ti–V–Al, Ti–V–Sn and Ti–V–Al–Sn were selected in this work. In this paper, the previous results of Young's modulus [4] are also demonstrated, and we discuss the mechanical properties of α′ Ti alloys in relation to the effects of the alloying element and content, with a comparison with those of equilibrium (α + β) Ti alloys. Based on these results, this paper then discusses the possibilities of new type α′ Ti alloys and a microstructural control technique that utilizes the α′ martensite phase.

2. Experimental procedures

(Ti–(4–25) mass% V)–(0–6) mass% Al alloys and (Ti–(4–25) mass% V)–(0–6) mass% Sn alloys were prepared by arc melting in an argon atmosphere using high purity Ti, V, Al and Sn. The Al or the Sn was added to Ti–V alloys so that the ratio of the Ti-to-V content was kept constant at Ti–(4–25 mass%) V. For example, 2, 4, or 6 mass% Al was added to (Ti–4 mass% V), keeping (Ti–4 mass% V) constant. The impurity content was about 600 mass ppm for oxygen and 80 mass ppm for nitrogen in the Ti–V–Al and Ti–V–Sn alloys. Similarly, Ti–(0, 2, 4, 6) mass% Al–6 mass% V–2 mass% Sn alloys were prepared by arc melting in an argon atmosphere. Since the changes in weight before and after arc melting were less than 50 mg, the alloy compositions will be denoted hereafter by their nominal compositions.

Arc-melted buttons with a weight of about 90 g were homogenized at 1423 K for 86.4 ks in an argon atmosphere and hot rolled at 1123 K to a thickness of 5 mm and 7 mm. The hot-rolled plates were homogenized at 1423 K for 86.4 ks, followed by cooling in an argon atmosphere (Hereafter, these homogenized samples will be called 1423 K HT). In addition, the hot-rolled plates were solution treated at 1223 K (for near β – (α + β)-type Ti–V–Al and Ti–V–Sn alloys), 1323 K (for near α – (α + β)-type Ti–V–Al and Ti–V–Sn alloys) or 1373 K (for Ti–(0, 2, 4, 6) mass% Al–6 mass% V–2 mass% Sn alloys) for 7.2 ks in an evacuated quartz tube, and then quenched in ice water (Hereafter, quenched samples will be called STQ). The STQ samples were cold rolled to a final thickness of 1 mm (Hereafter, the cold rolled samples will be called CR). The STQ sample with a composition of (Ti–12%V)–2%Al was heat treated at 823 K for 86.4 ks, followed by cooling in an Ar atmosphere to obtain the equilibrium (α + β) phase (Hereafter, this heat treated sample will be called 823 K HT).

Microstructures were identified by X-ray diffraction (XRD), optical microscopy (OM), and transmission electron microscopy (TEM). The dynamic Young's modulus at room temperature was measured by the free resonance vibration method using a sample with dimensions of 10 mm × 50 mm × 1 mm. Strength and elongation to fracture at room temperature were evaluated by tensile testing at an initial strain rate of $1.5 \times 10^{-4}\ s^{-1}$. In addition, strain rate dependence on 0.2% proof stress, ultimate tensile strength, and elongation to fracture at room temperature were evaluated by tensile testing at strain rates of $1.5 \times (10^{-2}, 10^{-3}, 10^{-4}$ and $10^{-5})\ s^{-1}$. Cold-rolling ability was evaluated by determining the limited cold-rolling reduction at which a cracking on the surface of the plate first appeared under cold rolling. In this evaluation, the samples, which were solution treated and quenched in ice water, were cold rolled from a thickness of 5 mm or 7 mm.

3. Result and discussions

3.1. Microstructures of Ti–V–Al and Ti–V–Sn alloys (STQ and HT)

Fig. 1 shows the optical micrographs of STQ alloys of (a) (Ti–4%V)–1%Al, (b) (Ti–4%V)–4%Al, (c) (Ti–12%V)–2%Al, (d) (Ti–8%V)–4%Sn, and (e) (Ti–12%V)–6%Sn. It can be seen that direct quenching in ice water from 1323 K or 1223 K results in an almost fully acicular martensitic structure for all alloys. The constituent phases of the quenched samples analyzed by XRD and TEM observation are summarized in a Ti–V–Al ternary phase diagram in Fig. 2(a) and a Ti–V–Sn ternary phase diagram in Fig. 2(b), in which the compositional ranges are V from 0 to 30 mass% and (Al or Sn) from 0 to 6 mass%, respectively. From the XRD profiles and TEM observation, it was determined whether the constituent phase was α′ (H.C.P.) martensite or α (H.C.P.) phase by confirming the absence of β formation in the microstructure, a needle-like microstructural characteristic, and the formation of a $\{1\,0\,\bar{1}\,1\}$ twin in a variant. The formation of a $\{1\,0\,\bar{1}\,1\}$ twin under quenching in Ti alloy is recognized as being caused by the martensitic transformation of β/α′ [5]. In Fig. 2, we can note the suppression of athermal ω formation with an increase in the alloy content of Sn or Al, and the larger region of single phase of α′, α″ and β for Ti–V–Al alloy as compared with Ti–V–Sn alloy. It can also be seen that the addition of A1 to Ti–V alloy is more effective for suppressing the athermal ω formation than the addition of Sn. This difference in the efficiency of the suppression of ω phase can be expected to affect the martensitic transformation. That is, the addition of Al, which strongly retards athermal ω formation, promotes the martensitic transformation, thereby resulting in expansion of the single phase region (α′, α″ and β) (Fig. 2(a)). Concerning the phase constituent in quenched Ti–V–(Al or Sn) alloy, the results are in good agreement with the previous reports of Maeda and Flower [6], and Ohyama and Nishimura [7].

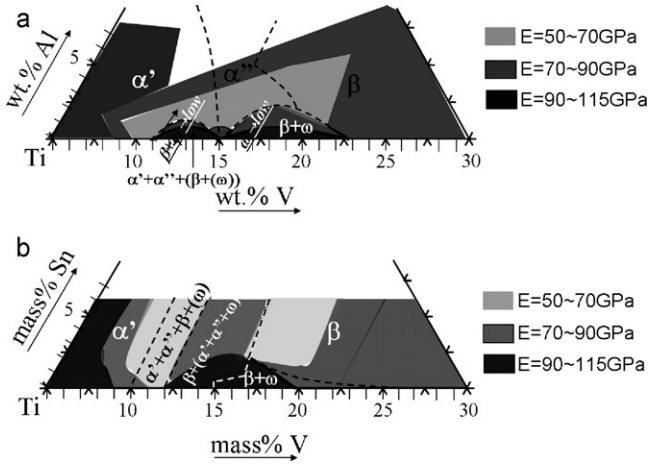

Fig. 2. Young's modulus of STQ (a) Ti–V–Al, and (b) Ti–V–Sn alloys illustrated in ternary phase diagrams.

3.2. Young's modulus of Ti–V–Al and Ti–V–Sn alloys (STQ)

In Fig. 2(a) and (b), the Young's modulus in Ti–V–Al alloy (STQ) and Ti–V–Sn alloy (STQ) is also illustrated. In the compositional

region in which primary constituent phase is α′ or β, it can be seen that a low Young's modulus (50–70 GPa) is obtained by increasing the addition of Al or Sn associated with the suppression of athermal ω formation. We also find that the Young's modulus increases with an increase in the V content in the primary constituent phase of β, while by contrast, it does so with a decrease in the V content in the primary constituent phase of α′. This thus shows the tendency for the Young's modulus to increase with the stabilization of the α′ phase or β phase, accompanying the decrease or increase of V content, and a low Young's modulus is obtained in the compositional region where the phase stability becomes low. Comparing the Young's modulus in the Ti–V–Al alloy system with that in the Ti–V–Sn alloy system in the metastable β compositional region, we note lower values in the Ti–V–Al alloy system than in the Ti–V–Sn alloy system. This tendency is attributed to the difference in alloying effect, in that the addition of Al as compared to Sn is more effective for the suppression of athermal ω formation. To date, Young's modulus in Ti alloys has been discussed in relation to crystallographic structure [8,9]. In metastable β-type Ti alloys, several authors have indicated that the low Young's modulus was caused by lattice instability. Moreover, in (α + β) type Ti–6%Al–4%V alloy, Lee and Welsch have also pointed out that the decrease in Young's modulus with changes of the heat treatment conditions is related to the effects of the instability of the β phase and its derivative martensite phases [10]. Summarizing the effects of composition and the alloying element on the Young's modulus in Ti–V–Al and Ti–V–Sn alloy systems with consideration of the above interpretations, Young's modulus strongly depends on phase stability, that is, a low Young's modulus is obtained by suppression of the athermal ω phase and in the compositional region where the stability of constituent phase becomes low. In other words, a high Young's modulus greater than 70 GPa is obtained by increasing the phase stability, independent of the primary constituent phases of α′, α″ and β.

3.3. Cold-rolling ability of Ti–V–Al and Ti–V–Sn alloys (STQ)

Fig. 3 summarizes the cold-rolling ability of (a) Ti–V–Al alloy (STQ) and (b) Ti–V–Sn alloy (STQ), and the constituent phases are also illustrated. Regarding the cold-rolling ability of Ti–V–Sn alloy (Fig. 3(b)), an excellent cold-rolling ability of more than 80% that is independent of the phase constituent can be seen. This result implies that α′ martensite with an H.C.P. structure in Ti–V–Sn alloy shows excellent ductility as compared with the equibrium α phase with an H.C.P. structure. In general, Ti alloys are classified as α, (α + β), and β types, depending on their crystallographic structure. They can be further subdivided into near-α – (α + β), near-β – (α + β), and metastable β-type alloys, depending on the alloy composition. In Ti–V–Al alloy (STQ), it should be noted that the cold-rolling ability drastically decreases with increasing Al content in α′ phase in the compositional region of near-α – (α + β), while excellent cold-rolling ability with a more than 75% reduction can be seen in the constituent phases of α′ in the compositional region of near-β – (α + β), α″ and β. These results indicate that the addition of Al retards ductility at room temperature. Next, we discuss the excellent cold-rolling ability in α′ phase with an H.C.P. structure in relation to the effect of the addition of Al and the active deformation mode at room temperature.

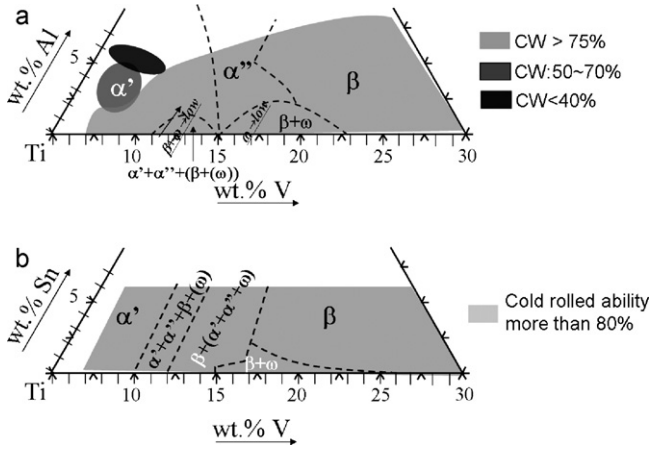

Fig. 3. Cold-rolling ability of STQ (a) Ti–V–Al, and (b) Ti–V–Sn alloys illustrated in ternary phase diagrams.

3.4. Strength and deformation characteristics in Ti–V–Al alloy

3.4.1. α′ martensite Ti–V–Al alloy with composition in near-α – (α + β) alloy

Fig. 4 shows the stress–strain curves after tensile testing at room temperature of (a) 1323 K STQ (Ti–4%V)–(1, 2, 4)%Al alloys, and (b) 1373 K STQ Ti–(0, 2, 4, 6)%Al–6%V–2%Sn alloys, which consist of fully α′ martensite. In Fig. 4(a) and (b), one can observe an increase in strength with increasing Al content, no apparent work hardening under plastic deformation, and a little decrease in elongation to fracture with increasing Al content.

Fig. 5 shows the cold-rolling ability of (a) STQ (Ti–4%V)–(1, 2, 4)%Al alloys, and (b) STQ Ti–(0, 2, 4, 6)%Al–6%V–2%Sn alloys. In Fig. 5(a), the results for the cold-rolling ability of (Ti–4%V)–(1, 2, 4)%Al alloys that have a lamella (α + β) microstructure are also

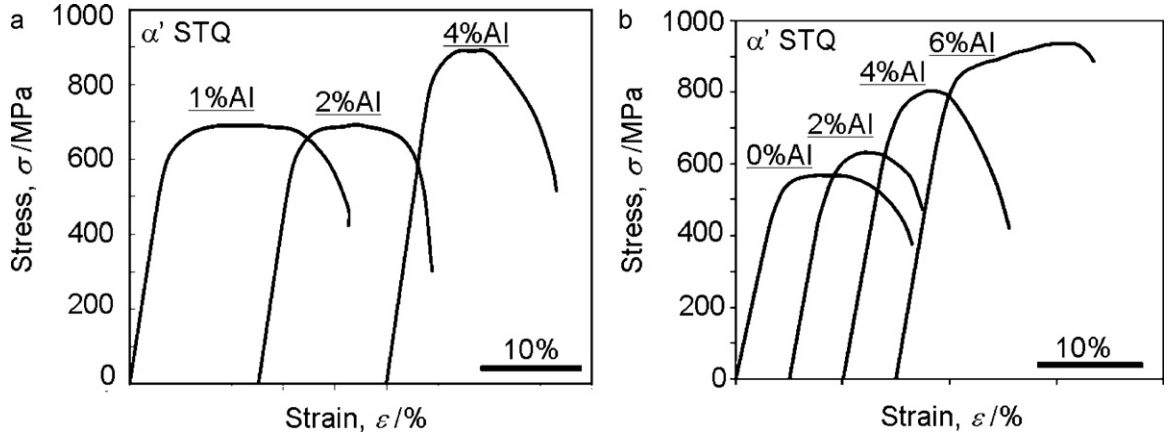

Fig. 4. Stress–strain curves of (a) (Ti–4%V)–(1, 2, 4)%Al alloys (1323 K STQ composed of α′) and Ti–(0, 2, 4, 6)%Al–6%V–2%Sn alloys (1373 K STQ composed of α′).

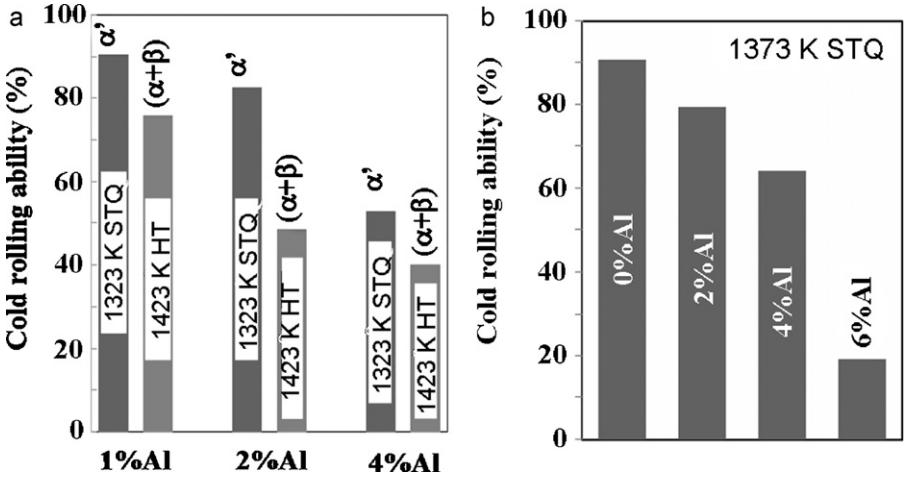

Fig. 5. Cold-rolling ability of (a) (Ti–4%V)–(1, 2, 4)%Al alloys (1323 K STQ composed of α′ and 1423 K HT composed of (α + β)), and (b) Ti–(0, 2, 4, 6)%Al–6%V–2%Sn alloys (1373 K STQ composed of α′).

shown. These results reveal a drastic decrease in cold-rolling ability with increasing Al content, and a higher degree of cold-rolling ability in the α′ phase as compared with the (α + β) phase for all alloys of (Ti–4%V)–(1, 2, 4)%Al and Ti–(0, 2, 4, 6)%Al–6%V–2%Sn.

The deformation characteristics of pure α-Ti have been widely studied [11–13]. There have been reports that the active deformation modes of pure α Ti are slip systems with Burgers vectors of *a*-type ($a/3\ \langle 1\,1\,\bar{2}\,0\rangle$), which can glide in prismatic, basal, and first-order pyramidal planes, and ⟨*c* + *a*⟩-type ($a/3\ \langle 1\,1\,\bar{2}\,3\rangle$, which can glide in first and second-order pyramidal planes, as well as some twinning systems [14]. Among these deformation modes, the prismatic gliding of *a*-type dislocations is the primary deformation mode, in which the deformation is controlled by the motion of the screw segments. The addition of Al to pure Ti retards the activation of the twinning of $\{1\,\bar{1}\,0\,2\}$ in tension and $\{\bar{1}\,2\,\bar{1}\,2\}$ in compression [15]. In addition, in α-Ti alloys, the dislocation sub-structures become less uniform and eventually exhibited quite planar configurations with increasing Al content [16]. The increase in the planarity of the slip in α-Ti alloys with increasing Al content is caused by a short range order. Fig. 6 shows TEM bright field images of 5% tensile-deformed (a) STQ Ti–2%Al–6%V–2%Sn alloy, and (b) STQ Ti–6%Al–6%V–2%Sn alloy consisting of a single α′ phase. In the alloy containing 2% A1 (Fig. 6(a)), a homogenous deformation substructure with straight-type dislocations that are aligned parallel to the ⟨*a*⟩ directions of $[1\,1\,\bar{2}\,0]$ and $[2\,\bar{1}\,\bar{1}\,0]$ (in Variant 1) and the dislocation loops is seen in the α′ variants. On the other hand, in the alloy containing 6% Al (Fig. 6(b)), dislocations in the α′ phase are arranged in planar configurations parallel to the ⟨*a*⟩ direction of $[\bar{2}\,1\,1\,0]$. The deformation microstructure, as shown in Fig. 6, shows that increasing Al content leads to a dislocation substructure that has a planar configuration in the α′ phase as well as in the equilibrium α phase. This planar configuration of dislocations (Fig. 6(b)) with increasing Al content is considered to be caused by the occurrence of short range order in the α′ phase, resulting in a decrease in ductility and cold-rolling ability (Figs. 4 and 5). Moreover, the higher ductility in the α′ phase as compared with the lamella (α + β) microstructure (Fig. 5) might be attributed to the following two causes. One is caused by the difference of solute Al content

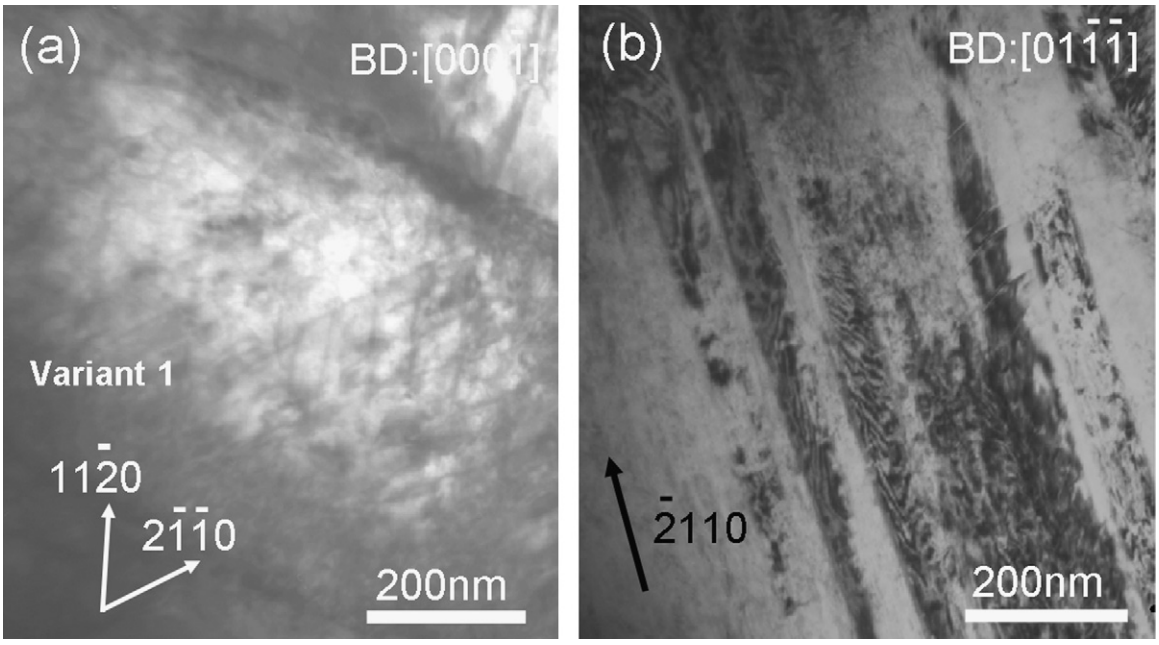

Fig. 6. TEM bright field images of tensile-tested STQ alloys at a strain of 5% in (a) Ti–2%Al–6%V–2%Sn and (b) Ti–6%Al–6%V–2%Sn.

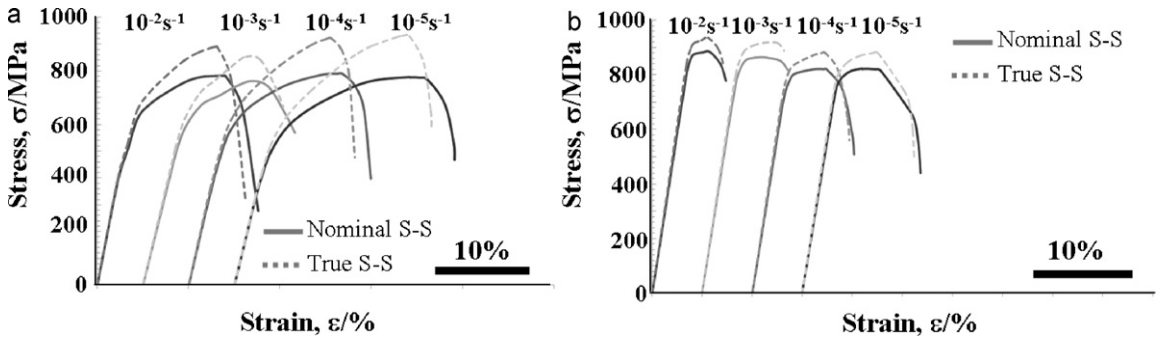

Fig. 7. Stress–strain curves demonstrated by nominal type- and true type-curves in (Ti–12%V)–2%Al alloy ((a) STQ composed of α′ phase, and (b) 823 K HT composed of lamellar (α + β) microstructure) after tensile testing as a function of strain rate.

into H.C.P. phases between the equilibrium α phase in the lamella (α + β) microstructure and α′ phase. The other cause is the possibility of activation of a complementary deformation mode which is observed in α′ phase with a composition near β – (α + β), as stated below.

3.4.2. α′ martensite Ti–V–Al alloy with composition in near-β – (α + β) alloy

Fig. 7 shows the stress–strain curves demonstrated by nominal type- and true type-curves in (Ti–12%V)–2%Al alloy of (a) STQ consisting of α′ phase, and (b) 823 K HT that has a lamellar (α + β) microstructure, after tensile testing as a function of strain rate. A higher work-hardening ratio and ductility can be seen in the STQ sample than in the 823 K HT. Also, a larger region of shrinkage is observed in STQ than in 823 K HT (Fig. 7). Fig. 8 shows the strain-rate dependence on (a) strength (0.2% proof stress and ultimate tensile strength), and (b) elongation to fracture in (Ti–12%V)–2%Al alloy (STQ and 823 K HT). Here, the strain-rate sensitivity parameter of *m* is illustrated in Fig. 8. In the STQ sample as compared to the 823 K HT sample, a lower the 0.2% proof stress and similar values in ultimate tensile strength, independent of strain rate, can be seen. Furthermore, a higher *m* value in the STQ sample can also be noted. This implies a difference between the deformation characteristics of the α′ phase and (α + β) phase, though the absolute magnitude of *m* is quite low in both phases. The difference between the deformation characteristics of the α′ phase and (α + β) phase will be discussed in later (in this paper). According to the *m* value of the β-type Ti alloy [17], similar values (*m* = 0.026 for Ti–6.8%Mo–4.5%Fe–1.5%Al and *m* = 0.033 for Ti–10%V–4.5%Fe–1.5%Al) were shown as compared to the *m* value of α′ (Ti–12%V)–2%Al alloy.

In order to determine the stability of the plastic flow in tension at room temperature, it is useful to use following the strain-hardening parameter, γ (denoted by formula (1)). This strain hardening parameter, γ, is defined as follows.

$$\gamma = \frac{1}{\sigma}\frac{d\sigma}{d\varepsilon} \tag{1}$$

In this formula (1), plastic deformation proceeds stably when $\gamma \geqq 1$. Plastic instability in tension commences when γ becomes less than 1-*m* (where *m* is the strain-rate sensitivity parameter). This indicates the formation of necking, which extends over the entire gauge length [18]. In the region from $\gamma = 1 - m$ to $\gamma = (1/2) - m$, the quasi-stable flow terminates and localized necking commences, resulting in eventual failure [19]. The strain-hardening parameter, γ, in (Ti–12%V)–2%Al alloy as a function of true strain, deformed at different strain rates, is shown in Fig. 9(a) for STQ and (b) for 823 K HT. In the STQ sample composed of fully α′ martensite, the amount of strain under a stable plastic flow decreases with increasing strain rate. However, it can be seen that the STQ sample exhibits stable plastic flow independent of the strain rate. In contrast, a rapid decrease of γ to negative values after yielding is observed at all strain rates for the 823 K HT sample composed of (α + β) (Fig. 9(b)). This result indicates that a larger region of stable plastic flow is obtained in the α′ phase than in (α + β) phase. In β Ti alloys of Ti–6.8%Mo–4.5%Fe–1.5%Al and Ti–10%V–4.5%Fe–1.5%Al, plastic deformation undergoes quasi-stable flow immediately after yielding [17]. These β-type alloys exhibit deformation behavior accompanied by planar slip, thereby leading to quasi-stable plastic flow under plastic deformation. Thus, these results imply that the α′ phase possesses as excellent a cold-work ability as the β phase.

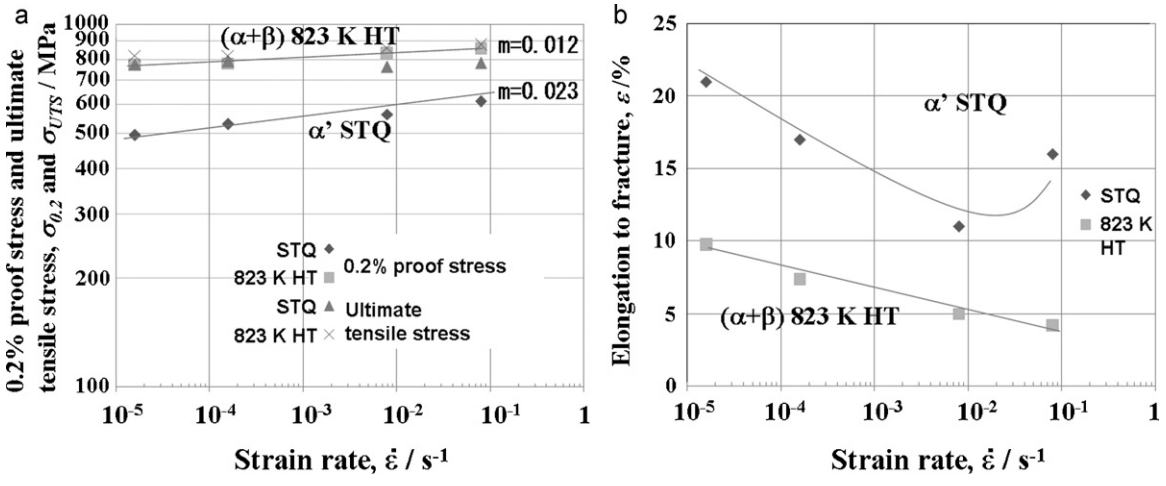

Fig. 8. Strain rate dependence on (a) strength (0.2% proof stress and ultimate tensile stress), and (b) elongation to fracture in (Ti–12%V)–2%Al alloy (STQ and 823 K HT).

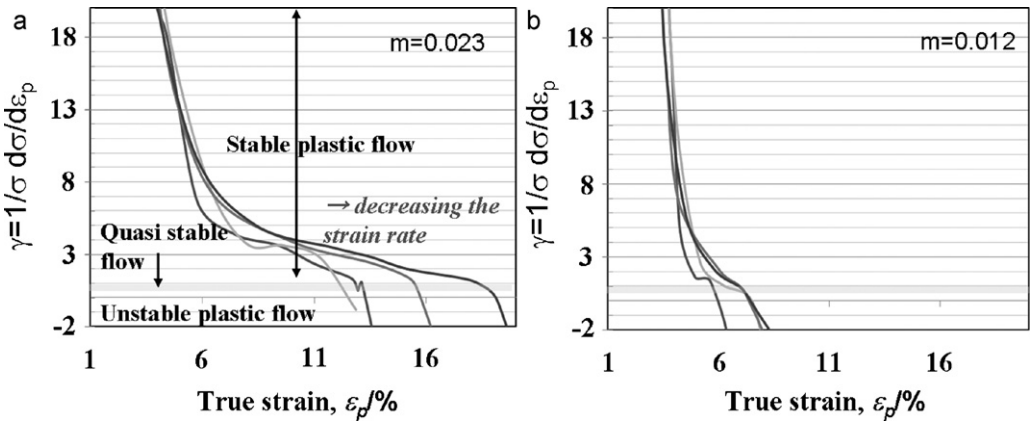

Fig. 9. Strain hardening parameter, γ, in (Ti–12%V)–2%Al alloy as a function of true strain deformed at different strain rates ((a) STQ and (b) 823 K HT).

Fig. 10 shows the surface morphologies of tensile-deformed (Ti–12%V)–2%Al alloy ((a) STQ and (b) 823 K HT) at a plastic strain of 7%. Localized slip bands are inhomogenously distributed on the surface of the 823 K HT sample, as shown by the arrays in Fig. 10(b). On the other hand, such localized slip bands cannot be seen in the STQ sample (Fig. 10(a)). This difference in surface morphology after tensile testing supports the stable manner of the α′ phase under plastic deformation, while the unstable manner in (α + β) phase is as described above (in Fig. 9).

To characterize the deformation characteristic in the α′ phase, TEM observation of tensile-deformed (Ti–12%V)–2%Al alloys (STQ in Fig. 11 and 823 K HT in Fig. 12) at a strain of 7% was performed. $\{1\,0\,\bar{1}\,1\}$ twins in the martensite variant, indicated by a solid line, were confirmed (Fig. 11(a)). As mentioned in Section 3.1, the $\{1\,0\,\bar{1}\,1\}$ twin is recognized as being formed during the martensitic transformation of β/α′ [5]. Therefore, we cannot judge whether the observed $\{1\,0\,\bar{1}\,1\}$ twin (Fig. 11(a)) was induced by martensitic transformation or deformation. However, the fraction of the

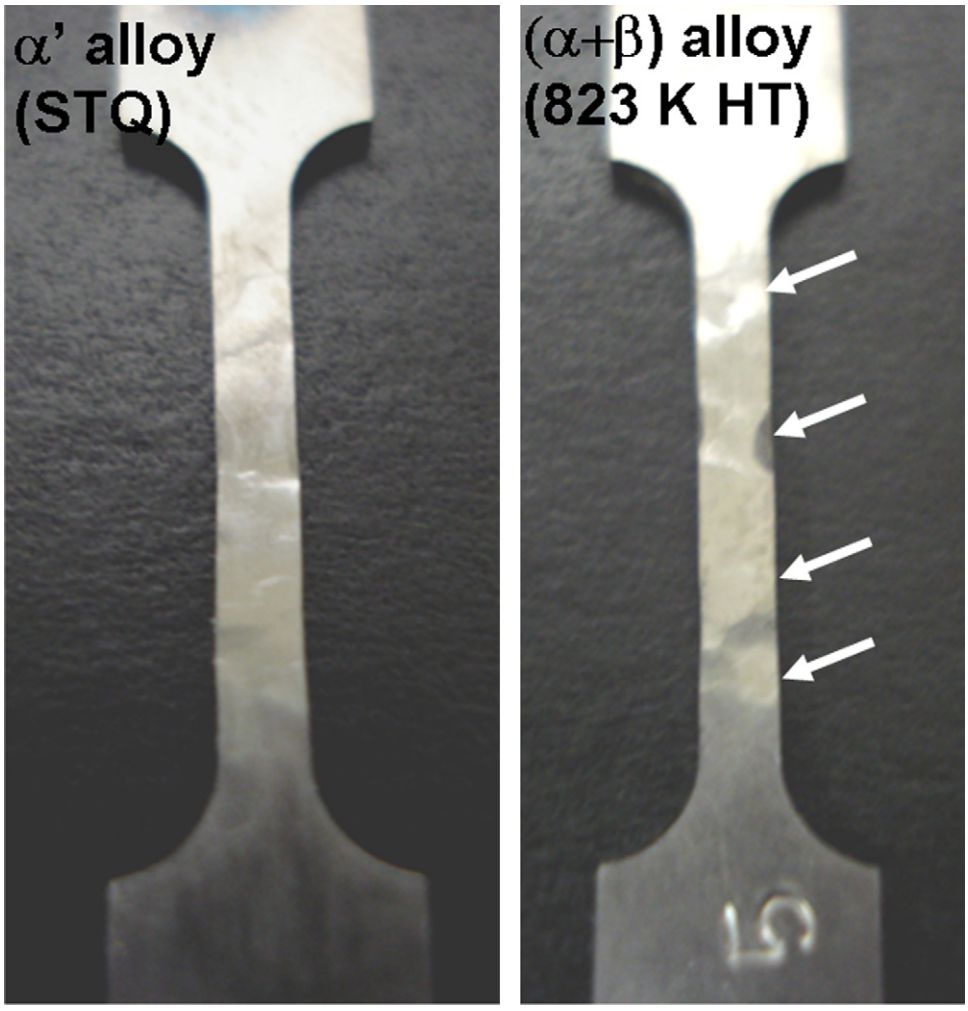

Fig. 10. Surface morphologies of tensile-deformed (Ti–12%V)–2%Al alloy (a) STQ and (b) 823 K HT) at a strain of 7%.

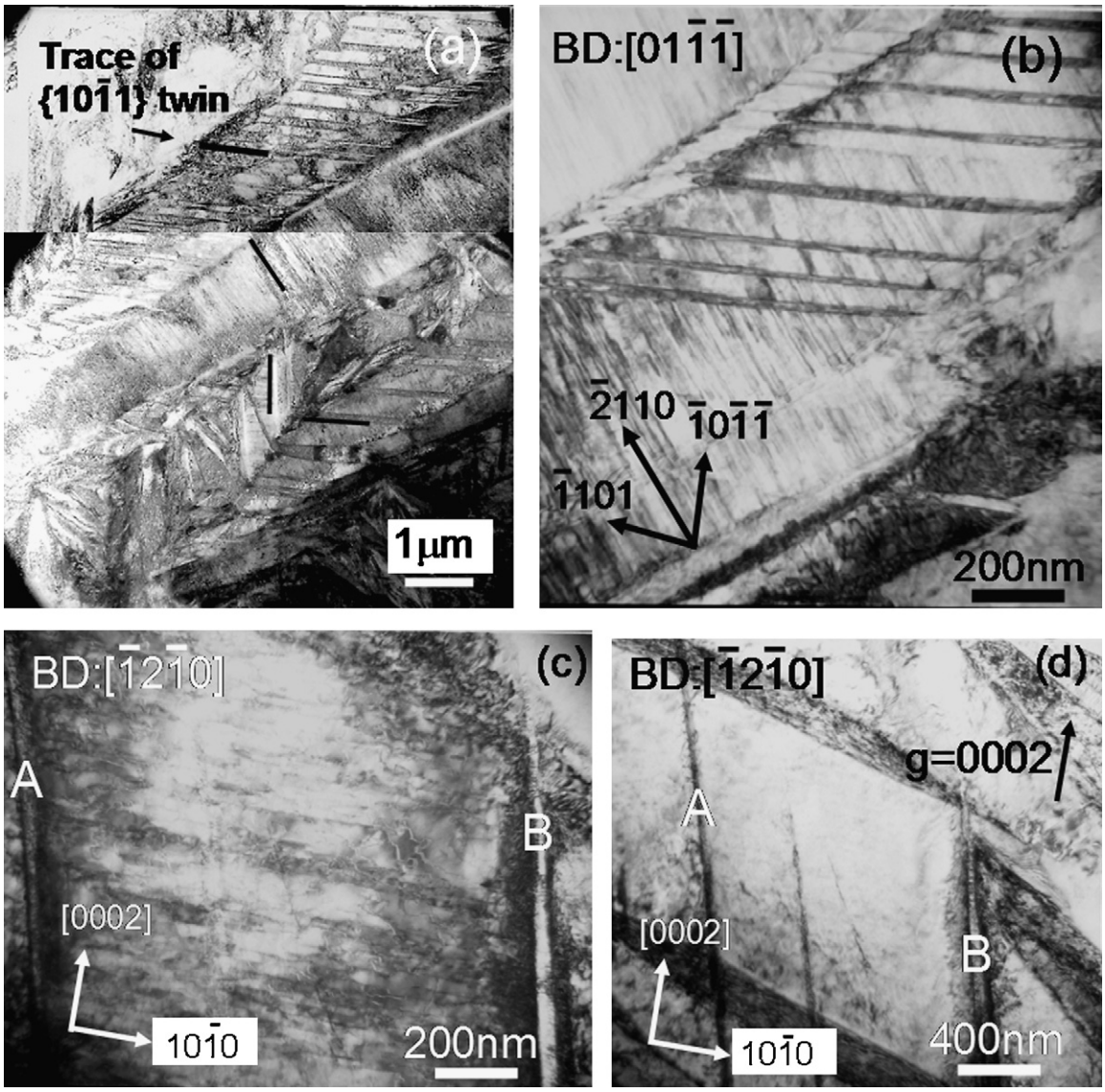

Fig. 11. TEM bright field images of tensile-deformed (Ti–12%V)–2%Al alloy (STQ composed of α′) at a strain of 7%.

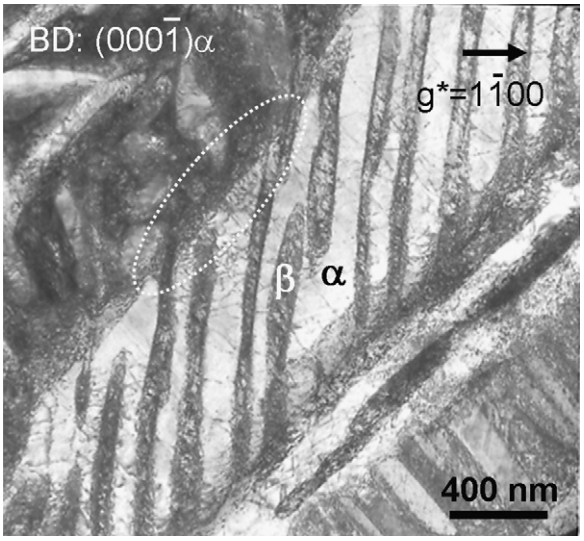

Fig. 12. TEM bright field image of tensile-deformed (Ti–12%V)–2%Al alloy (823 K HT composed of (α + β)) at a strain of 7%.

{1 0 $\bar{1}$ 1} twin after deformation apparently increases, as compared with the microstructure of the as-quenched (Ti–12%V)–2%Al alloy. Furthermore, twinning systems other than the {1 0 $\bar{1}$ 1} twin cannot be confirmed in the deformed microstructure (Fig. 11(a)). This implies the activation of the {1 0 $\bar{1}$ 1} twin under deformation in the STQ sample. As is well known, the primary deformation modes in commercially pure α-Ti are the prismatic ⟨*a*⟩ slip of {0 1 $\bar{1}$ 0} ⟨$\bar{2}$ 1 1 0⟩, and the minor deformation modes of {0 0 0 1} ⟨1 1 $\bar{2}$ 0⟩ slip (basal ⟨*a*⟩ slip), {1 1 $\bar{2}$ 2} ⟨$\bar{1}$ $\bar{1}$ 2 3⟩ slip (⟨*a* + *c*⟩ slip), and {1 1 $\bar{2}$ 1}, and {1 1 $\bar{2}$ 3} and {1 1 $\bar{2}$ 4} twinning [20]. Also, based on the magnitude of CRSS (critical resolved shear stress) for twinning and slip, Paton and Backofen pointed out that the {1 0 $\bar{1}$ 1} twin and basal ⟨*a*⟩ slip are difficult to activate under deformation as compared with other twinning and slip systems [21]. Therefore, the formation of the {1 0 $\bar{1}$ 1} twin after deformation would be caused by the process of rearrangement of the martensite variants, which is a typical characteristic of thermo-elastic martensitic transformation. In the α martensite variant, many dislocation lines with a straight characteristic can be seen (Fig. 11(b) and (c)). Fig. 11(d) was TEM bright field image that was taken in the same region with Fig. 11(c) using the reflection of $g = 0002$. The traces of A and B in Fig. 11(c) and

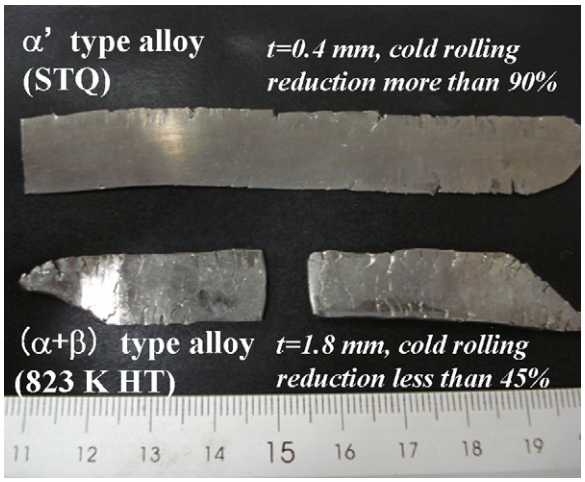

Fig. 13. Appearance of cold-rolled plates of (Ti–12%V)–2%Al alloy (STQ and 823 K HT).

(d) show the traces corresponding to the $\{1\,0\,\bar{1}\,1\}$ twin. It is noted that dislocation segments are straight and parallel to basal-plane trace as shown in Fig. 11(c), and are out of contrast when $g = 0002$ as shown in Fig. 11(d). Therefore, based on the $g \cdot b = 0$ criterion, all straight dislocations are determined to consist of an $\langle a \rangle$ Burgers vector gliding on the basal plane (Fig. 11(c) and (d)). This result indicates the activation of basal $\langle a \rangle$ slip as well as $\{1\,0\,\bar{1}\,1\}$ twinning under deformation in the α′ phase in (Ti–12%V)–2%Al alloy. As stated above, the primary deformation mode in α and (α + β) Ti alloys is the prismatic $\langle a \rangle$ slip of $\{0\,1\,\bar{1}\,0\}$ $\langle \bar{2}\,1\,1\,0 \rangle$. Unfortunately, the CRSS of the slip system and twinning system of α′ phase in Ti alloy has not been reported. In our previous report, based on the development of the texture of α′ phase under cold rolling, we speculated that there could be a frequent occurrence of $\langle a + c \rangle$ slip with an increase in strain under deformation [2]. On the basis of the above results, we can speculate that basal $\langle a \rangle$ slip and $\{1\,0\,\bar{1}\,1\}$ twinning are activated in the initial stage of plastic deformation, and $\langle a + c \rangle$ slip begins to be activated with increasing strain under cold deformation.

Fig. 12 shows a TEM micrograph of (Ti–12%V)–2%Al alloy (823 K HT) that has been tensile-deformed at a strain of 7%. In Fig. 12, the white area corresponds to the α phase, and the black area to the β phase. It can be seen that the dislocations in the α phase are rectilinear (Fig. 12). Moreover, we note that the dislocations have accumulated particularly at the interface of the lamella colonies, indicated by a white dotted line in Fig. 12, rather than at the α/β interface in the lamella. Castany et al. have pointed out that the α/β interface in a lamella structure acts as a source of emission sites for screw dislocations having an $\langle a \rangle$ Burgers vector; it does not, however, act as an obstacles to the dislocation motion in Ti–6%Al–4%V alloy [22]. These dislocation configurations are similar to the results obtained for 823 K HT (Fig. 12), which demonstrates the similarity in the manner of deformation of Ti–6%Al–4%V alloy and 823 K HT in (Ti–12%V)–2%Al alloy. As a consequence, such a dislocation characteristic in the (α + β) phase (Fig. 12) would be the cause of the inhomogenous deformation characteristic (Fig. 9(b)).

In a comparison between the cold-rolling ability of the α′ phase and (α + β) phase in (Ti–12%V)–2%Al alloy, Fig. 13 shows the appearance of cold-rolled plates of STQ and 823 K HT. Cracking is apparent in the 823 K HT plate after cold-rolling at a reduction of 45%; in contrast, excellent cold-rolling ability of more than 90% is confirmed for STQ. From these results for cold-rolling ability (Fig. 13), we can see the excellent cold-working ability in the α′ phase compared to the (α + β) phase in (Ti–12%V)–2%Al alloy.

3.5. The possibility of α′ type Ti alloys for a new type of Ti structural material

Summarizing the results obtained in this work, we can understand that the addition of Al to a Ti–V alloy system leads to an inhomogenous deformation microstructure with a planar dislocation substructure under plastic deformation in the α′ phase as well as the equilibrium α phase, thereby retarding its ductility at room temperature. However, Ti–V–Al alloys with a low Al content were found to exhibit markedly superior ductility in the α′ phase as compared to the equilibrium (α + β) phase. In other words, in compositional region that exhibit a deformation mictrostructure without a planar-slip mode caused by the Al addition, α′ Ti alloys exhibit an excellent ductility due to activation of the deformation modes of basal $\langle a \rangle$ slip, $\{1\,0\,\bar{1}\,1\}$ twinning and $\langle a + c \rangle$ slip. This result also demonstrates that high cold-working ability can be obtained by utilizing the α′ phase. Regarding the strength, in fact, Ti–V–Al alloys with a low Al content exhibits the lower 0.2% proof stress of 500–650 MPa as compared to the strength in the present engineering Ti alloys as shown in Figs. 4(a) and 8(a). However, it is expected that this lower strength can be improved easily by controlling the grain size of microstructure. Cold-rolling of α′ Ti alloy results in a refined equiaxed dislocation cell microstructure with a grain size less than 100 nm, and leads to a high degree of strengthening of more than 1000 MPa [1]. In addition, it is possible to control of the mechanical properties of Young's modulus and strength by low-temperature heat treatment [1,23]. These results also suggest a new type of microstructural controlling technique for high functionalizing using α′ martensite in the production of industrial Ti alloys.

4. Summary

In this study, a systematic evaluation of the microstructures and mechanical properties of Ti–V–(Al, Sn) alloys with a α′ martensitic structure was conducted by changing the alloy content and heat treatment conditions. The obtained results are summarized as follows.

(1) In as-quenched Ti–V–Al alloys consisting of α′ martensite with compositions of near-α – (α + β), cold-rolling ability drastically decreases from a reduction of more than 75% to less than 40% with increasing Al content (from 0 mass% to 6 mass%). While, the alloys with the constituent phases of α′ in the compositional region of near-β – (α + β), α″ and β, exhibit the excellent cold-rolling ability with a reduction of more than 75%. On the other hand, excellent cold-rolling ability with a reduction of more than 80% is seen in as-quenched Ti–V–Sn alloys, which is independent of the phase constituents.
(2) Young's modulus strongly depends on phase stability, that is, a low Young's modulus is obtained by suppression of the athermal ω phase and in a compositional region in which the stability of the constituent phase becomes low. In other words, a high Young's modulus of more than 70 GPa is obtained by increasing the phase stability, independent of the primary constituent phases of α′, α″ and β.
(3) In α′ martensite Ti–Al–6%V–2%Sn alloy with a composition of near-α – (α + β) that was tensile-deformed at a strain rate of 5%, a homogenous deformation substructure is seen in alloy with a low Al content. In contrast, the dislocation substructure exhibits a planar configuration in alloy with high Al content. This change in deformation substructure by increasing the Al content would cause the low ductility. On the other hand, plastic deformation is found to be proceeded via the activation of the basal $\langle a \rangle$ slip and $\{1\,0\,\bar{1}\,1\}$ twin with a homogenous deformation

substructure in α′ martensite Ti–V–Al alloy with a composition of near-β – (α + β). This deformation mode in α′ phase would result in the high ductility as compared with the equilibrium (α + β) phase.

Acknowledgment

This work was partially supported by a Grant from the New Energy and Industrial Technology Development Organization (NEDO, 08E51003d).

References

[1] H. Matsumoto, T. Watanabe, S. Hanada, Mater. Sci. Eng. A448 (2007) 39–48.
[2] H. Matsumoto, A. Chiba, S. Hanada, Mater. Sci. Eng. A486 (2008) 503–510.
[3] Y. Murakami, O. Izumi, T. Nishimura, Titanium'95 Science and Technology, The Institute of Materials, London, 1996, pp. 1403–1422.
[4] H. Matsumoto, S. Watanabe, N. Masahashi, S. Hanada, Metall. Trans. A 37 (2006) 3239–3249.
[5] J.C. Williams, R. Tagart, D.H. Polonis, Metall. Trans. 1 (1970) 2265–2270.
[6] T. Maeda, H.M. Flower, in: P. Lacombe, R. Tricot, G. Beranger (Eds.), Proceedings of 6th World Conference on Titanium, Les Editions de Physique, Paris, June 6–9, 1988, pp. 1589–1594.
[7] H. Ohyama, T. Nishimura, in: P.A. Blenkinsop, W.J. Evans, H.M. Flower (Eds.), Proceedings of Eighth World Conference on Titanium, Birmingham, UK, October 22–26, 1995, pp. 2273–2280.
[8] A.W. Bowen, Proceedings of Fourth International Conference on Titanium "TITANIUM'80", 1980, pp. 1317–1326.
[9] Z. Fan, Scripta Metall. Mater. 29 (1993) 1427–1432.
[10] Y.T. Lee, G. Welsch, Mater. Sci. Eng. A128 (1990) 77–89.
[11] A. Akhtar, E. Teghtsoonian, Metall. Trans. A6 (1975) 1105–1113.
[12] S. Naka, A. Lasalmonie, P. Costa, L.P. Kubin, Philos. Mag. A57 (1988) 717–740.
[13] S. Farenc, D. Caillard, A. Couret, Acta Metall. Mater. 41 (1993) 2701–2709.
[14] S. Zaefferer, Mater. Sci. Eng. A344 (2003) 20–30.
[15] N.E. Paton, J.C. Williams, G.Q. Rauscher, in: N.I. Jaffee, N. Qromisel (Eds.), The Science, Technology and Applications of Titanium, 1970, p. 1049.
[16] J.C. Williams, G. Luetjering, Titanium'80 Science and Technology Proceedings of Fourth International Conference on Titanium, Kyoto Japan, May 10–22, 1980, pp. 671–681.
[17] A. Bhattacharjee, P. Ghosal, A.K. Gogia, S. Bhargava, S.V. Kamat, Mater. Sci. Eng. A 452–453 (2007) 219–227.
[18] G.E. Dieter, Mechanical Metallurgy, 3rd ed., McGraw-Hill Inc., New York, 1988, pp. 275–24.
[19] A.K. Ghosh, in: S.S. Hecker, A.K. Ghosh, H.L. Gegel (Eds.), Formability, Analysis, Modeling and Experimentation, AIME, 1978, pp. 14–28.
[20] S. Hanada, Tetsu-to-Hagane 76 (1990) 495–502 (in Japanese).
[21] N.E. Paton, W.A. Backofen, Trans. AIME 245 (1969) 1369–1370.
[22] P. Castany, F. Pettinari-Sturmel, J. Crestou, J. Douin, A. Coujou, Acta Mater. 55 (2007) 6284–6291.
[23] H. Matsumoto, K. Kodaira, A. Chiba, J. Jpn. Inst. Met. 72 (2008) 989–996.